Article

Diagnosing destabilization risk in global land carbon sinks

🔴 Check for updates

Marcos Fernández-Martínez[1,2,3 ✉], Josep Peñuelas[2,4], Frederic Chevallier[5], Philippe Ciais[5], Michael Obersteiner[6,7], Christian Rödenbeck[8], Jordi Sardans[2,4], Sara Vicca[1], Hui Yang[5], Stephen Sitch[9], Pierre Friedlingstein[10], Vivek K. Arora[11], Daniel S. Goll[5], Atul K. Jain[12], Danica L. Lombardozzi[13], Patrick C. McGuire[14] & Ivan A. Janssens[1]

Global net land carbon uptake or net biome production (NBP) has increased during recent decades[1]. Whether its temporal variability and autocorrelation have changed during this period, however, remains elusive, even though an increase in both could indicate an increased potential for a destabilized carbon sink[2,3]. Here, we investigate the trends and controls of net terrestrial carbon uptake and its temporal variability and autocorrelation from 1981 to 2018 using two atmospheric-inversion models, the amplitude of the seasonal cycle of atmospheric CO_2 concentration derived from nine monitoring stations distributed across the Pacific Ocean and dynamic global vegetation models. We find that annual NBP and its interdecadal variability increased globally whereas temporal autocorrelation decreased. We observe a separation of regions characterized by increasingly variable NBP, associated with warm regions and increasingly variable temperatures, lower and weaker positive trends in NBP and regions where NBP became stronger and less variable. Plant species richness presented a concave-down parabolic spatial relationship with NBP and its variability at the global scale whereas nitrogen deposition generally increased NBP. Increasing temperature and its increasing variability appear as the most important drivers of declining and increasingly variable NBP. Our results show increasing variability of NBP regionally that can be mostly attributed to climate change and that may point to destabilization of the coupled carbon–climate system.

Positive carbon–climate feedbacks have the potential to accelerate climate change and might compromise the attainability of ambitious climate targets such as those set by the Paris agreement[4]. Terrestrial ecosystems are key to the functioning of the global carbon (C) cycle and have increased their productivity and net C uptake during recent decades primarily owing to CO_2 fertilization and forest regrowth[1,5–7]. However, land-use change, nutrient limitations and increasing droughts and fires are constraining this potential to sequester C[8–11]. Identifying processes that might destabilize net land C uptake (or net biome production, NBP) is of paramount importance for understanding and managing the global C cycle.

Destabilization is the process of losing stability: that is, when a system loses its ability to return to equilibrium following a disturbance. A symptom of this may be increased variability, as the system spirals away from its current equilibrium point towards a new one. Destabilization of a dynamical system is usually accompanied by concomitant increases in temporal variability and autocorrelation (the correlation between consecutive time steps (AR1), also related to reduced resilience[2]) when AR1 is already positive because anomalous states of the system create ripples that can get amplified through time rather than compensated as when AR1 is negative. Consequently, increasing temporal variability and autocorrelation have been shown to be potential early-warning signals for abrupt shifts in ecosystems[2,3,12,13]. To date, changes in NBP temporal variability and autocorrelation have not yet been investigated even though increased stress and changes in the frequency and intensity of extreme weather events are likely to alter the temporal patterns of NBP[14–16] because of (1) a cumulative negative effect of extreme events on ecosystem functioning, (2) increasing climate variability and (3) decreasing ecosystem resilience due to increased stress. We, thus, hypothesized that regions experiencing increasing trends in climate variability will also experience increasing variability in their NBP and that increase in variability may indicate that a destabilization of the net land C uptake is occurring. This finding could serve as an early-warning signal for abrupt shifts in the functions of an

ecosystem[2] that might lead to regime shifts in the Earth's biosphere[17,18]. Even if these changes do not occur at the global scale, increasing temporal variability and autocorrelation in several regions of the globe (for example, Amazon basin and boreal ecosystems with permafrost) could have a profound impact on the global C balance and a knock-on effect on other ecosystem functions.

Climate is the primary control of NBP in terrestrial ecosystems worldwide in space and time[19,20], together with soil nutrient availability[10,21], atmospheric nitrogen (N) deposition, land use and management and increasing atmospheric CO_2 (ref.[1]). Generally, gross C fluxes (such as photosynthesis and respiration) are larger in the tropics where high temperature coincides with sufficient precipitation to enable long growing seasons. However, net C uptake tends to be higher in temperate regions because of higher nutrient availability[19,21–23]. Nutrient availability and N deposition have indeed been shown to increase net land C uptake[21,22]. Another factor believed to be important in determining ecosystem functioning is plant biodiversity[24]. A large body of evidence indicates its role in promoting ecosystem productivity and stability[25,26]. Plant biodiversity, however, has been included far less in studies of ecosystem C cycling, presumably due to the difficulty of acquiring good data on species diversity. The few studies that included biodiversity, however, showed relatively modest correlations with C fluxes[27–29]. The role of biodiversity in the global terrestrial NBP has not yet been explored even though the Earth's biosphere is losing biodiversity at an unprecedented speed[30] and those changes are expected to alter ecosystem functioning.

The aim of this study was to quantify the trends in global NBP and its intradecadal temporal variability (quantified by the proportional variability (PV) index[31,32]) and autocorrelation (AR1) to see whether changes in these variables suggest that NBP at global or regional scales is being destabilized. We further tested whether regions with increasing variability and AR1 in NBP showed differential trends in annual NBP. We additionally investigated the spatial correlation between NBP metrics and plant biodiversity (derived from a global map of plant species richness[33]), atmospheric total N deposition[34], climate[35] and land use (land-use harmonization[2] maps). To realize these objectives, we used estimates of NBP derived from the two longest CO_2 atmospheric inversions (CAMS and CarboScope) and the amplitude of the seasonal cycle of atmospheric CO_2 derived from nine monitoring stations distributed from south to north of the Pacific Ocean for 1981 to 2018. We additionally compared these results with the output from an ensemble of 12 dynamic global vegetation models (TRENDY) to explore how well these state-of-the-art models predict the spatial and temporal patterns in NBP simulated by atmospheric-inversion models.

Temporal patterns of net land C uptake

Global NBP derived from atmospheric inversions increased from 5.6 ± 2.0 gC m^{-2} y^{-1} during 1981–1990 (mean ± standard error) to 13.8 ± 1.4 gC m^{-2} y^{-1} during 2009–2018 over the global land area, excluding Antarctica (Fig. 1). This represents an overall increase of 145% and an annual linear increase of 0.24 ± 0.08 gC m^{-2} y^{-2} ($P < 0.001$). Both atmospheric inversions used (CAMS and CarboScope) identified annual increases in NBP (Supplementary Figs. 1 and 2, 0.32 ± 0.09 and 0.18 ± 0.09 gC m^{-2} y^{-2}, respectively, $P < 0.001$, $n = 38$). The positive trend in NBP shown by inversions is similar in magnitude to the trend identified by the TRENDY ensemble (0.10 ± 0.07 gC m^{-2} y^{-2}, $P < 0.001$; 147% when comparing the periods 1981–1990 and 2009–2018). Both observations and models, however, showed a flattening trend during the last decade (Fig. 1c). In parallel with the increased NBP throughout the entire study period and in agreement with previous literature[36,37], the amplitude of the seasonal atmospheric CO_2 concentration increased by 0.027 ± 0.004 ppm y^{-1} ($P < 0.001$, 16.6% during the study period) (Supplementary Fig. 3a).

Interannual NBP variability (NBP_{PV}) derived from the combination of atmospheric inversions increased globally by 7.2% over the entire period ($P < 0.001$) (Fig. 1f) (CAMS 14.9%, $P < 0.001$; CarboScope −1.3%, $P < 0.001$). The origin of the discrepancy between the inversions remains unclear. Although the inversions differ in whether they use a growing number of measurement stations (CAMS) or a constant station set (CarboScope), the discrepancy is unlikely to be related to this because a test inversion with a growing station set in the CarboScope inversion did not yield an increase in NBP_{PV}. Temporal variability in the amplitude of the seasonal atmospheric CO_2 concentration also increased (by 35%, $P < 0.001$) during the study period (Supplementary Fig. 3b). TRENDY NBP did not simulate this increase in variability, showing a negative trend of −1.7% in NBP_{PV} similar to that from the CarboScope inversion.

Global NBP_{AR1} significantly decreased over time for NBP derived from atmospheric inversions (Fig. 1i) and for the average monthly CO_2 concentrations across the Pacific Ocean (Supplementary Fig. 3c). TRENDY NBP_{AR1} also showed a significant negative trend representing a reduction of 2.9% over the study period. Trends of contrasting sign, however, were significant amongst atmospheric measurement stations and atmospheric inversions (CAMS −10.0%, $P < 0.001$; CarboScope 4.7%, $P < 0.001$). Several regions showed increases in the temporal autocorrelation between consecutive months (NBP_{AR1}) derived from atmospheric inversions that are of a similar magnitude (about 0.2 over three decades) to those previously suggested to precede abrupt shifts in climate datasets and simulations[2,3]. Further information on how changes in NBP_{PV} and NBP_{AR1} may affect annual NBP and their limitations can be found in Supplementary Information Section 1.

Our analyses identified several regions of potential concern given their concomitant increase in NBP_{PV} and NBP_{AR1} (Fig. 2a), such as eastern Africa, the Mediterranean region, the west coasts of North and Central America, India and southeast Asia. Regions with increasing NBP_{PV} and NBP_{AR1} had statistically lower NBP and experienced a much less pronounced increase in NBP over time (0.15 ± 0.06 gC m^{-2} y^{-1}, $P < 0.001$) compared to regions where NBP_{PV} and NBP_{AR1} decreased (0.73 ± 0.12 gC m^{-2} y^{-1}, $P < 0.001$) (Fig. 2b–d and Supplementary Fig. 4). Stronger increases in NBP over regions with decreasing NBP_{PV} and NBP_{AR1}, compared to those in which they increased, were also evident from both atmospheric inversions when analysed separately (Supplementary Fig. 5).

Global temperature and precipitation increased during the study period (Supplementary Fig. 6a,d) even though there was considerable spatial variability in those trends (Supplementary Fig. 7a,d). Temperature and precipitation interannual variability, however, decreased significantly at the global scale, despite the reported increase in extreme weather[14]. Temporal autocorrelation of monthly temperature and precipitation, instead, increased slightly, albeit significantly only for temperature. A concomitant increase in temporal variability and autocorrelation of temperature was evident in several regions (for example, Eurasia, Australia and Central America) but those were not so obvious for precipitation (Supplementary Fig. 8).

Controls of NBP, variability and autocorrelation

NBP, derived from atmospheric inversions, had a concave-down parabolic relationship with biodiversity (Fig. 3), increasing from low to intermediate values of biodiversity and decreasing at high biodiversity (Supplementary Fig. 9a). Our analyses also identified a significant positive interaction between biodiversity and N deposition accounting for NBP. The concave-down relationship between biodiversity and NBP included mainly positive NBP values across regions with high atmospheric N deposition (850 mgN m^{-2} y^{-1}) and mainly negative NBP values at low atmospheric N deposition (100 mgN m^{-2} y^{-1}) (Supplementary Fig. 9a). Similarly, the positive correlation between N deposition and
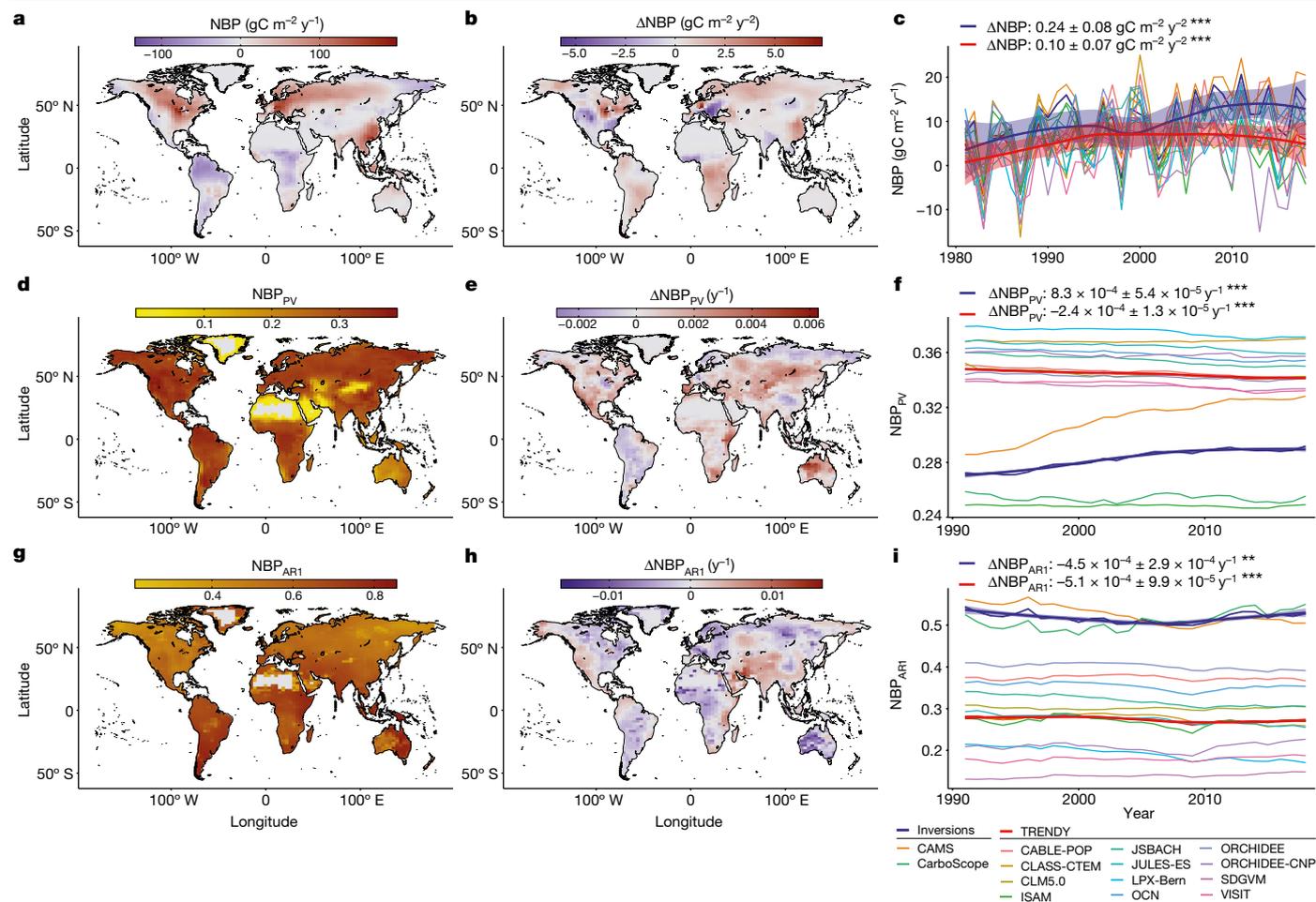
Fig. 1 | Global distribution of NBP, NBP_PV and NBP_AR1 and their trends from 1981 to 2018. a, The average global distribution of NBP (positive values indicate C sinks) derived from CAMS and CarboScope atmospheric inversions. **b,c**, The temporal trends in NBP (ΔNBP) (**b**) and the temporal change in NBP derived from atmospheric inversions and 12 DGVMs (TRENDY) (**c**). **d,e** and **f**, **g,h** and **i** mimic **a**, **b** and **c**, respectively, for NBP_PV and NBP_AR1 calculated over an 11-year moving window. Thick lines in **c**, **f** and **i** represent smooth trends estimated with a local regression (shaded areas show the standard error of the trend) and the coefficients at the top of the panels indicate robust Theil–Sen's slopes (± standard error of the slope) with their corresponding *P* values, estimated using the non-parametric Wilcoxon Mann–Whitney rank sum test. Values in **c**, **f** and **i**, represent spatially weighted global means. **P < 0.01; ***P < 0.001.

NBP was stronger in regions with higher plant biodiversity (Supplementary Fig. 9b). Opposite relationships emerged when analysing TRENDY NBP.

NBP_PV derived from inversions showed a concave-down parabolic relationship with plant biodiversity, peaking at intermediate to high values of biodiversity (Supplementary Fig. 9d). We also found an interaction between plant biodiversity and N deposition in their relationship with NBP_PV: the relationship between NBP_PV and biodiversity differed between areas receiving low N deposition and areas receiving high N deposition (Supplementary Fig. 9d). No relationship between N deposition and NBP_PV was found in regions with high biodiversity, whereas a positive relationship occurred in regions with low biodiversity (Supplementary Fig. 9e). Interannual variabilities in temperature and precipitation were positively correlated with NBP_PV (Fig. 3). In this case, the patterns for the TRENDY ensemble and the inversion models matched very well. Again, NBP_AR1 derived from inversions had a concave-down parabolic relationship with biodiversity (Supplementary Fig. 9g) but here no interaction occurred between the effects of biodiversity and N deposition, which was negatively correlated with NBP_AR1. NBP_AR1 was also positively correlated with temperature AR1, the only result that match those from TRENDY NBP_AR1 (Supplementary Fig. 9i). Results

emerging from individual atmospheric inversions (CAMS and CarboScope) mostly coincided with those reported above (Supplementary Fig. 10).

Spatial variability in the trends of NBP, NBP_PV and NBP_AR1 derived from atmospheric inversions were all correlated with N deposition, climate and land use (Fig. 3 and Supplementary Fig. 11). The estimated effects of land use and land-use change, however, were generally lower than those from N deposition and climate, hence accounting for a smaller proportion of the change at the global scale. N deposition was positively correlated with the trends in NBP and negatively with trends in NBP_PV and NBP_AR1 (Supplementary Fig. 11). Warmer regions were more likely than colder regions to have decreasing trends in NBP and increasing temperatures contributed to decreasing NBP (Supplementary Fig. 11b,c). Regions with the strongest increases in NBP_PV were spatially associated with low increases in annual temperature (Supplementary Fig. 11e). Increases in NBP_PV were also found to be more likely in regions showing increases in temperature temporal variability (Supplementary Fig. 11f). Increasing NBP_AR1 was more likely in regions with increasing temperatures (Supplementary Fig. 11h) and with increasing temporal autocorrelation of precipitation (Fig. 3). Our analyses using TRENDY reproduced the abovementioned findings well for trends in NBP and
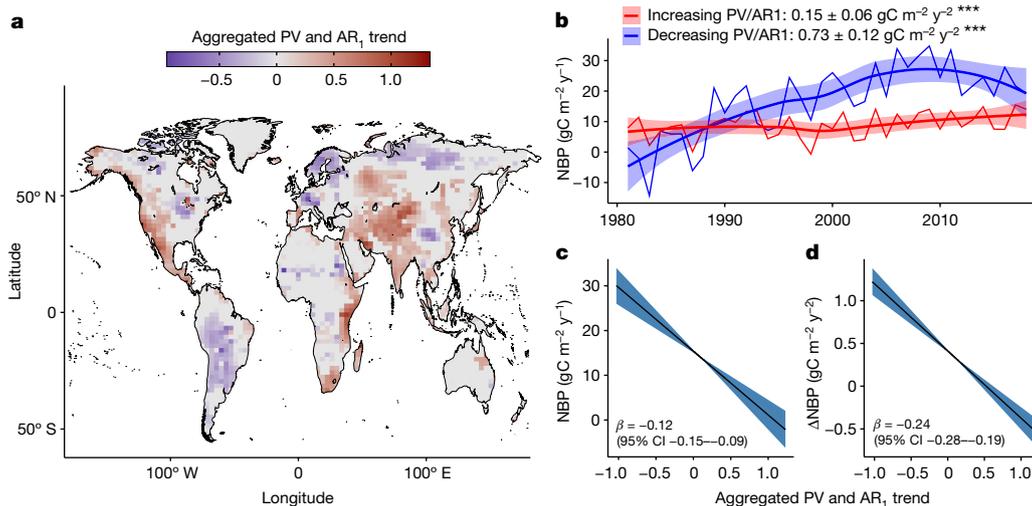
Fig. 2 | Regions with concomitantly increasing NBP_{PV} and NBP_{AR1} present lower NBP and a lower increase of NBP over time. a, Regions of the world where concomitant increases (red) and decreases (blue) in NBP_{PV} and NBP_{AR1} have occurred during the study period. Regions with contrasting trends in NBP_{PV} and NBP_{AR1} appear in grey. **b**, The aggregated annual mean NBP of regions with increasing (red) and decreasing (blue) NBP_{PV} and NBP_{AR1} (see Supplementary Fig. 4 for information on their global contribution). Smooth trends were estimated with a local regression (shading indicates the standard error of the trend) and the coefficients at the top of the panel indicate robust Theil–Sen's slopes (± standard error of the slope) and their associated significance (***$P < 0.001$), estimated using the non-parametric Wilcoxon Mann–Whitney rank sum test. **c,d**, The spatial relationship of NBP (**c**) and trends in NBP (ΔNBP) (**d**) with the aggregated trend of NBP_{PV} and NBP_{AR1}. Coefficients are standardized and include the 95% credible intervals. See Methods for details on how the aggregated trend of NBP_{PV} and NBP_{AR1} was calculated.

NBP_{AR1} but not for NBP_{PV}. Again, results from individual atmospheric inversions were similar to those reported here (Supplementary Fig. 10). Warm regions presenting a concomitant increase in temperature temporal variability and autocorrelation (symptoms of destabilization) were more likely to be correlated with similar changes in NBP variability and AR1 and those results were well supported by both atmospheric inversions and their combination (Supplementary Fig. 12). Additionally, regions with higher N deposition, larger proportions of forested areas and lower crops were related to concomitantly decreasing NBP_{PV} and NBP_{AR1}.

Biodiversity, N deposition and net C uptake

NBP derived from atmospheric inversions provided correlational evidence indicating that plant biodiversity may be playing an important role in regulating regional variation in the land C balance and in its temporal variability. TRENDY models, instead, do not include biodiversity in their parameterization and, hence, any spurious relationship is necessarily driven by factors other than biodiversity. The spatial relationship between biodiversity and NBP clearly differed between atmospheric inversions and TRENDY (Supplementary Fig. 9a), hence suggesting that the reported effect of biodiversity when analysing atmospheric inversions may emerge because of a mechanistic effect. The emerging relationship between biodiversity and NBP_{PV} derived from atmospheric inversions, however, was very similar to the one emerging from TRENDY, which suggests that factors other than biodiversity may be driving this relationship. The positive relationship between biodiversity and NBP_{AR1} found here has never been reported before and further research is needed to understand the mechanisms behind this relationship.

The concave-down parabolic relationships of biodiversity with NBP and NBP_{PV} differ from most biodiversity–productivity and stability relationships reported in the literature: positive asymptotic for productivity and negative for variability[38,39]. This difference in the biodiversity–NBP relationship may result from two opposing ecosystem processes, photosynthesis and respiration, because both are likely to be enhanced by biodiversity[27,40,41]. The concave-down relationship would then suggest that the positive effect of biodiversity on respiration overshadows the positive effect of photosynthesis in regions with high biodiversity. However, our biodiversity data, as in similar studies[39], were restricted to species richness and did not include information on species abundance, their individual contribution to NBP or traits to allow the calculation of actual species diversity or functional diversity, often better indicators of ecosystem functioning than is species richness[42]. Unfortunately, this information is not available at the global scale. Including actual diversity in future analyses could lead to different results to those reported here. Additionally, future efforts are needed to understand how biodiversity loss, not included here, will impact global carbon balance.

Interestingly, our analyses indicated that the effect of biodiversity on NBP depended on atmospheric N deposition and vice versa (Fig. 3). The effect of atmospheric N deposition on NBP was mainly positive but was stronger in regions with higher biodiversity, further supporting the premise that biodiversity promotes ecosystem functions such as N uptake[43]. Regions with higher N deposition also had larger increases in NBP over time (Supplementary Fig. 11a), supporting previous findings suggesting a stronger CO_2 fertilization effect in regions with higher N deposition[1]. On the other hand, N deposition was negatively related to trends in NBP_{PV}, NBP_{AR1} and the aggregated trend of NBP_{PV-AR1} (Supplementary Fig. 12), which suggests that N addition may ameliorate nutrient imbalances derived from increasing atmospheric CO_2 concentrations[8] and prevent ecosystem functioning from becoming more variable.

Climate and changing land C uptake

Our results clearly indicate that NBP decreased in regions with warm climates and in which warming has been most pronounced (Supplementary Fig. 11). These findings support results from previous studies[1] and further suggest that increasing droughts and heat waves limit C sequestration by terrestrial ecosystems[44]. Our analyses revealed that higher NBP_{PV} and NBP_{AR1} and their trends were associated, respectively, with climates showing higher and increasing temporal variability and
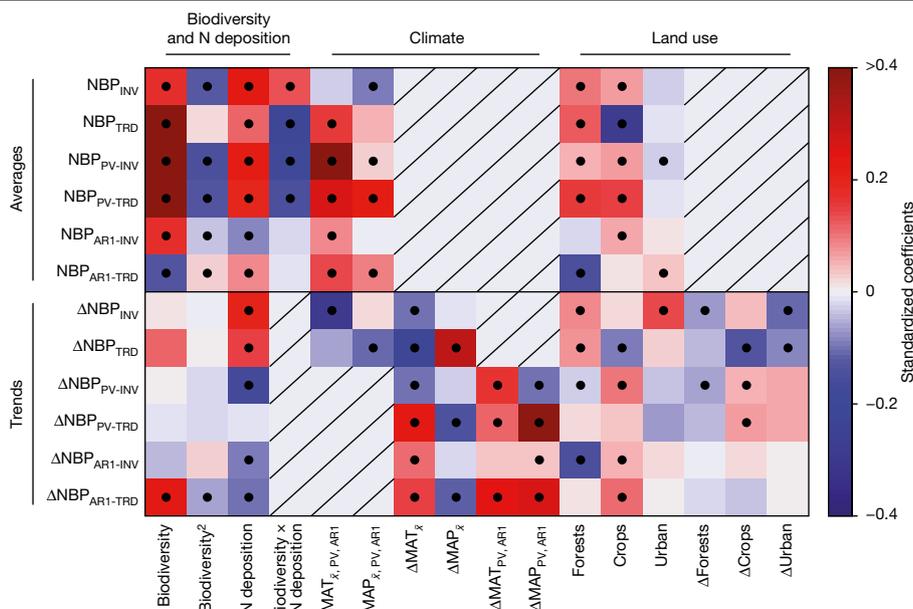
Fig. 3 | Contribution of biodiversity, N deposition, climate and land use to NBP, NBP_PV, NBP_AR1 and their trends. The colour scale indicates the strength of the relationship (standardized β coefficients) between each predictor (bottom) and the response variable (left). Black dots indicate that 95% of the posterior distributions differed from 0. Biodiversity was fitted as a second-order polynomial to account for nonlinearities (biodiversity + biodiversity^2; the second term indicates the change in the slope in biodiversity as biodiversity increases). Hashed areas indicate relationships not included in the regression models. See Methods for further information on model fitting. INV and TRD indicate the averages for all atmospheric inversions (2) and DGVMs (12), respectively. Predictors $\mathrm{MAT}_{\bar{x},PV,AR1}$ and $\mathrm{MAP}_{\bar{x},PV,AR1}$ indicate mean, PV or AR1 metrics of MAT and MAP matching the metric of the response variable (for example, $\mathrm{NBP_{INV}} \approx \mathrm{MAT}_{\bar{x}}$; $\mathrm{NBP_{PV\text{-}INV}} \approx \mathrm{MAT_{PV}}$). The same applies for $\Delta\mathrm{MAT_{PV}}$, $\Delta\mathrm{MAT_{AR1}}$, $\Delta\mathrm{MAP_{PV}}$ and $\Delta\mathrm{MAP_{AR1}}$. Δ, trend in a given variable.

autocorrelation (Supplementary Fig. 9). We also found that concomitantly increasing trends in $\mathrm{NBP_{PV\text{-}AR1}}$ were positively related to increasing temperature variability and autocorrelation (Supplementary Fig. 12). These results support our initial hypothesis stating that climate change may be the main contributing factor for changing the temporal behaviour of land C sinks.

Implications of altered land C sinks

Compelling evidence from atmospheric inversions (Fig. 1) and the annual amplitude of the seasonal CO_2 cycle (Supplementary Fig. 3) suggest that global net land C uptake is now larger and, most likely, more variable than three decades ago, whereas its temporal autocorrelation ($\mathrm{NBP_{AR1}}$), instead, has significantly decreased. The increase in global NBP and the reduction in $\mathrm{NBP_{AR1}}$ were well identified by TRENDY NBP, including the evidence of a flattening trend in NBP during the last two decades. Our results for the increase in global NBP and a potential recent saturation are consistent with previous findings of increases in global productivity and NBP and a recent decline of the CO_2 fertilization effect[1,5,8,20]. Even though the main emerging spatial controls for CAMS and CarboScope atmospheric inversions in NBP were in agreement (Supplementary Figs. 8 and 10), trends at the global scale for $\mathrm{NBP_{PV}}$ and $\mathrm{NBP_{AR1}}$ were significantly different (Supplementary Fig. 13), which calls for caution in the interpretation of these results because of their uncertainty.

We observed a bifurcation of regions characterized by concomitant increases and decreases in $\mathrm{NBP_{PV}}$ and $\mathrm{NBP_{AR1}}$ (Fig. 2). This bifurcation relates to differences in their mean annual temperature, their increase in annual temperature, their average N deposition loads and their percentage of forests and crops (Supplementary Fig. 12). The observed increase in the variability and autocorrelation of net C uptake in several regions of the planet (Fig. 2a) is concerning because of the implications it can have for the stability of their ecosystems. First, increasing $\mathrm{NBP_{PV}}$ and $\mathrm{NBP_{AR1}}$ is indicative of increasing variability and reducing resilience[3,45] potentially in many ecosystem processes: from

photosynthesis and respiration[27] to cascading effects on animals and decomposers[46]. Second, an increase in variability in NBP implies that ecosystem C balance is less predictable over time, which is troublesome for projections of future climate change. Third, regions showing a combined increase in $\mathrm{NBP_{PV}}$ and $\mathrm{NBP_{AR1}}$ had a consistently lower NBP and lower increases in NBP than did regions where $\mathrm{NBP_{PV}}$ and $\mathrm{NBP_{AR1}}$ decreased (Fig. 2b–d), suggesting that these increases in $\mathrm{NBP_{PV}}$ and $\mathrm{NBP_{AR1}}$ reflect dynamical instability in the carbon system rather than some other cause (such as changes in the external forcing of the system). This destabilization may jeopardize future C sequestration. Our analyses, however, could not determine the mechanisms driving the observed changes in $\mathrm{NBP_{PV}}$ and $\mathrm{NBP_{AR1}}$. More importantly, we could not determine whether the observed increases in $\mathrm{NBP_{PV}}$ and $\mathrm{NBP_{AR1}}$ truly reflect dynamical instability in the carbon system, as opposed to some other cause, such as changes in the external forcing of the system (for example, increasing CO_2 emissions and N deposition). Hence, regions showing increased variability and autocorrelation should be monitored in detail to properly understand the mechanisms and consequences behind these changes given that increasing variability and autocorrelation have been shown to act as early-warning signals preceding abrupt phase transitions in simulations of ecosystem functioning[2,3]. The increase of $\mathrm{NBP_{PV}}$ and $\mathrm{NBP_{AR1}}$ in several regions should serve as an early-warning signal of potential future changes that the Earth's biosphere may be facing. Given the main role of climate change as a driver of these changes in their temporal behaviour, mitigating climate change is needed to prevent further unforeseen changes in land C sinks.

Online content

Any methods, additional references, Nature Portfolio reporting summaries, source data, extended data, supplementary information, acknowledgements, peer review information; details of author contributions and competing interests; and statements of data and code availability are available at https://doi.org/10.1038/s41586-023-05725-1.

1. Fernández-Martínez, M. et al. Global trends in carbon sinks and their relationships with CO_2 and temperature. *Nat. Clim. Change* **9**, 73–79 (2019).
2. Scheffer, M. et al. Early-warning signals for critical transitions. *Nature* **461**, 53–59 (2009).
3. Dakos, V. et al. Slowing down as an early warning signal for abrupt climate change. *Proc. Natl Acad. Sci. USA* **105**, 14308–14312 (2008).
4. Gasser, T. et al. Path-dependent reductions in CO_2 emission budgets caused by permafrost carbon release. *Nat. Geosci.* **11**, 830–835 (2018).
5. Zhu, Z. et al. Greening of the Earth and its drivers. *Nat. Clim. Change* **6**, 791–795 (2016).
6. Bastos, A. et al. Contrasting effects of CO_2 fertilization, land-use change and warming on seasonal amplitude of Northern Hemisphere CO_2 exchange. *Atmos. Chem. Phys.* **19**, 12361–12375 (2019).
7. Pugh, T. A. M. et al. Role of forest regrowth in global carbon sink dynamics. *Proc. Natl Acad. Sci. USA* **116**, 4382–4387 (2019).
8. Wang, S. et al. Recent global decline of CO_2 fertilization effects on vegetation photosynthesis. *Science* **370**, 1295–1300 (2020).
9. Peñuelas, J. et al. Assessment of the impacts of climate change on Mediterranean terrestrial ecosystems based on data from field experiments and long-term monitored field gradients in Catalonia. *Environ. Exp. Bot.* **152**, 49–59 (2018).
10. Terrer, C. et al. Nitrogen and phosphorus constrain the CO_2 fertilization of global plant biomass. *Nat. Clim. Change* **9**, 684–689 (2019).
11. Gatti, L. V. et al. Amazonia as a carbon source linked to deforestation and climate change. *Nature* **595**, 388–393 (2021).
12. Carpenter, S. R. & Brock, W. A. Rising variance: a leading indicator of ecological transition. *Ecol. Lett.* **9**, 311–318 (2006).
13. Dakos, V., Nes, E. H. & Scheffer, M. Flickering as an early warning signal. *Theor. Ecol.* **6**, 309–317 (2013).
14. Sillmann, J., Daloz, A. S., Schaller, N. & Schwingshackl, C. in *Climate Change* 3rd edn (ed. Letcher, T. M.) 359–372 (Elsevier, 2021).
15. Reichstein, M. et al. Climate extremes and the carbon cycle. *Nature* **500**, 287–295 (2013).
16. Wang, X. A two-fold increase of carbon cycle sensitivity to tropical temperature variations. *Nature* **506**, 212–215 (2014).
17. Barnosky, A. D. et al. Approaching a state shift in Earth's biosphere. *Nature* **486**, 52–58 (2012).
18. Buermann, W. et al. Climate-driven shifts in continental net primary production implicated as a driver of a recent abrupt increase in the land carbon sink. *Biogeosciences* **13**, 1597–1607 (2016).
19. Luyssaert, S. et al. CO_2 balance of boreal, temperate, and tropical forests derived from a global database. *Glob. Change Biol.* **13**, 2509–2537 (2007).
20. Peñuelas, J. et al. Shifting from a fertilization-dominated to a warming-dominated period. *Nat. Ecol. Evol.* **1**, 1438–1445 (2017).
21. Fernández-Martínez, M. et al. Nutrient availability as the key regulator of global forest carbon balance. *Nat. Clim. Change* **4**, 471–476 (2014).
22. Fernández-Martínez, M. et al. Spatial variability and controls over biomass stocks, carbon fluxes and resource-use efficiencies in forest ecosystems. *Trees Struct. Funct.* **28**, 597–611 (2014).
23. Ciais, P. et al. Five decades of northern land carbon uptake revealed by the interhemispheric CO_2 gradient. *Nature* **568**, 221–225 (2019).
24. Tilman, D., Lehman, C. L. & Thomson, K. T. Plant diversity and ecosystem productivity: theoretical considerations. *Proc. Natl Acad. Sci. USA* **94**, 1857–1861 (1997).
25. de Mazancourt, C. et al. Predicting ecosystem stability from community composition and biodiversity. *Ecol. Lett.* **16**, 617–625 (2013).
26. Sakschewski, B. et al. Resilience of Amazon forests emerges from plant trait diversity. *Nat. Clim. Change* **6**, 1032–1036 (2016).
27. Fernández-Martínez, M. et al. The role of climate, foliar stoichiometry and plant diversity on ecosystem carbon balance. *Glob. Change Biol.* **26**, 7067–7078 (2020).
28. Musavi, T. et al. Stand age and species richness dampen interannual variation of ecosystem-level photosynthetic capacity. *Nat. Ecol. Evol.* **1**, 0048 (2017).
29. Anderegg, W. R. L. et al. Hydraulic diversity of forests regulates ecosystem resilience during drought. *Nature* **561**, 538–541 (2018).
30. IPBES: Summary for Policymakers. In *The Global Assessment Report on Biodiversity and Ecosystem Services* (eds Díaz, S. et al.) 1–56 (IPBES, 2019).
31. Heath, J. P. Quantifying temporal variability in population abundances. *Oikos* **115**, 573–581 (2006).
32. Fernández-Martínez, M., Vicca, S., Janssens, I. A., Martín-Vide, J. & Peñuelas, J. The consecutive disparity index, D, as measure of temporal variability in ecological studies. *Ecosphere* **9**, e02527 (2018).
33. Kreft, H. & Jetz, W. Global patterns and determinants of vascular plant diversity. *Proc Natl Acad Sci USA* **104**, 5925–5930 (2007).
34. Ackerman, D. E., Chen, X. & Millet, D. B. Global nitrogen deposition (2°×2.5° grid resolution) simulated with GEOS-Chem for 1984–1986, 1994–1996, 2004–2006, and 2014–2016 (University of Minnesota, 2018); https://conservancy.umn.edu/handle/11299/197613.
35. Harris, I., Jones, P. D. D., Osborn, T. J. J. & Lister, D. H. H. Updated high-resolution grids of monthly climatic observations—the CRU TS3.10 Dataset. *Int. J. Climatol.* **34**, 623–642 (2013).
36. Graven, H. D. et al. Enhanced seasonal exchange of CO_2 by northern ecosystems since 1960. *Science* **341**, 1085–1089 (2013).
37. Wang, K. et al. Causes of slowing-down seasonal CO_2 amplitude at Mauna Loa. *Glob. Change Biol.* **26**, 4462–4477 (2020).
38. Tilman, D., Reich, P. B. & Knops, J. M. H. Biodiversity and ecosystem stability in a decade-long grassland experiment. *Nature* **441**, 629–632 (2006).
39. Liang, J. et al. Positive biodiversity–productivity relationship predominant in global forests. *Science* **354**, aaf8957–aaf8957 (2016).
40. Gessner, M. O. et al. Diversity meets decomposition. *Trends Ecol. Evol.* **25**, 372–380 (2010).
41. Peguero, G. et al. Fast attrition of springtail communities by experimental drought and richness–decomposition relationships across Europe. *Glob. Change Biol.* **25**, 2727–2738 (2019).
42. Díaz, S. & Cabido, M. Vive la différence: plant functional diversity matters to ecosystem processes. *Trends Ecol. Evol.* **16**, 646–655 (2001).
43. Cardinale, B. J. Biodiversity improves water quality through niche partitioning. *Nature* **472**, 86–91 (2011).
44. Ciais, P. et al. Europe-wide reduction in primary productivity caused by the heat and drought in 2003. *Nature* **437**, 529–533 (2005).
45. Scheffer, M. *Critical Transitions in Nature and Society* (Princeton University Press, 2009).
46. Ostfeld, R. & Keesing, F. Pulsed resources and community dynamics of consumers in terrestrial ecosystems. *Trends Ecol. Evol.* **15**, 232–237 (2000).

Article

Methods

Datasets

NBP and atmospheric CO_2 data. We obtained the global NBP data for 1981–2018 from the two atmospheric-inversion models that provided the longest time series: (1) the CAMS Greenhouse Gases Flux Inversions (https://ads.atmosphere.copernicus.eu/cdsapp#!/dataset/cams-global-greenhouse-gas-inversion)[47,48] v.18r3 and (2) the Jena CarboScope database v.s81oc_v2020 using a constant network of measurement stations (http://www.bgc-jena.mpg.de/CarboScope/)[49,50]. We also used NBP data from an ensemble of 12 dynamic global vegetation models (DGVMs) run with varying concentrations of atmospheric CO_2 and changing land uses and climates. Models compiled by the TRENDY project (v.8, models CABLE-POP, CLASS-CTEM, CLM5.0, ISAM, JSBACH, JULES-ES, LPX-BERN, OCN, ORCHIDEE, ORCHIDEE-CNP, SDGVM and VISIT) were used to test whether the DGVMs also identified the patterns from atmospheric inversions[51]. Previous studies indicate that DGVMs explain trends in NBP adequately; here, we test whether their emerging trends in NBP temporal variability and autocorrelation also match those from local observations or atmospheric inversions. We used model results from the simulation experiment S3, which was run with changing atmospheric CO_2, land use and climate (https://blogs.exeter.ac.uk/trendy/protocol/). We used monthly NBP estimates as the basis for all calculations in this study. We rescaled all atmospheric inversions, the TRENDY model outputs and the predictors to the same spatial resolution of the coarsest dataset for fitting the statistical models (see section below) (CAMS 3.75° × 1.875°).

We calculated average annual NBP per pixel, its temporal variability expressed as the PV index (NBP_{PV})[31,32] and its monthly temporal autocorrelation at lag 1 (NBP_{AR1}) for all of the abovementioned datasets. All three indices (NBP, NBP_{PV} and NBP_{AR1}) were calculated as the average for the entire period. The PV index is calculated as the mean PV amongst all possible combinations of values in a time series, following $PV = \frac{2\sum m}{n(n-1)}$, in which n indicates the length of the variable, m is calculated as $m = 1 - \frac{\min(z_i, z_j)}{\max(z_i, z_j)}$ and z represent the individual values used to calculate all the pairwise comparisons between the observations of the time series (for example, observation z_i versus observation z_j). When negative values occurred in a time series, we added a constant to the entire time series equivalent to the minimum absolute value plus one. Unlike other metrics of temporal variability, the PV index provides estimates of temporal variability that are independent of the mean of the time series and that have been proven to be robust even when comparing non-normally distributed datasets, thereby overcoming the mathematical drawbacks of similar variability indices such as the standard deviation or the coefficient of variation[52]. NBP_{PV} per pixel was estimated as the average of the interannual variabilities of all months (for example, $NBP_{PV} = \frac{NBP_{PV\,January} + [...] + NBP_{PV\,December}}{12}$). By using this method, NBP_{PV} reflects not only the interannual variability of the annual NBP but also the variation occurring amongst equal months across the years. Using this method, a year with average NBP yet with anomalously low NBP in one period offset by anomalously high NBP in another, would result in high interannual variability rather than low interannual variability. AR1 was estimated using the residuals of generalized additive models used to remove the trend and seasonal cycle of the data. In these models, the response variable was monthly NBP and the predictors were the month of the year (a factor of 12 levels) and the year, the last included as a spline smoothed term to account for nonlinear trends over time (Supplementary Fig. 14). We used the mgcv R package to fit the generalized additive models[53]. An 11-year moving average from NBP_{PV} and NBP_{AR1} per pixel was then calculated for all datasets to investigate trends in interannual variability and temporal autocorrelation. Our sensitivity analysis showed that our results were consistent despite the selection of different window lengths (7, 11 and 15 years, Supplementary Fig. 13 and Supplementary Table 1). Robust Theil–Sen trends[54] were then calculated for NBP, NBP_{PV} and NBP_{AR1} (ΔNBP, ΔNBP_{PV} and ΔNBP_{AR1}) per pixel using the mblm function in R[55]. Wilcoxon rank sum tests were performed to test the significance of the Theil–Sen trends. Even though we present results for both atmospheric inversions (CAMS and Carbo-Scope), we combined their results into one fusion dataset to further highlight those results for which both inversion models agreed (Supplementary Figs. 10 and 12). The combination was performed by calculating the average value of each of the abovementioned variables per pixel. We followed the same approach to provide a TRENDY dataset combining all simulations following similar studies[1].

Trends in average global NBP, NBP_{PV} and NBP_{AR1} (from 1981 to 2018 for NBP and from 1991 to 2018 for NBP_{PV} and NBP_{AR1}) were also estimated using the Theil–Sen approach. We combined both atmospheric inversions and the TRENDY simulations to provide the average results derived from atmospheric inversions and process-based models. In this case, the combination of products was performed by calculating the average between products per year and then estimating the temporal trends. We additionally calculated an aggregated metric of trends in NBP_{PV} and NBP_{AR1}. To do so, we first calculated the ratio between each value and the maximum absolute value of each of the variables (ΔNBP_{PV} and ΔNBP_{AR1}) and then we combined them by summing their relative values per pixel. Next, we selected those pixels in which both ΔNBP_{PV} and ΔNBP_{AR1} showed a positive trend and those which showed a negative trend and investigated their respective trends in NBP in the same way that we proceeded for global NBP.

Results obtained from the atmospheric inversions were compared with those from nine stations monitoring atmospheric CO_2 concentrations distributed from north to south of the Pacific Ocean that comprised the full period of this study. We selected this subset of monitoring stations to minimize the influence of anthropogenic emissions in the signal of atmospheric CO_2 concentration. These data were downloaded from the Scripps CO_2 programme: https://scrippsco2.ucsd.edu/data/atmospheric_co2/ (ref. [56]). We calculated the annual amplitude in CO_2 concentration (maximum minus minimum) using monthly data following refs. [20,36] as a proxy of the net global C uptake capacity. An 11-year moving average was then used to determine whether the annual amplitude of CO_2 concentrations, its PV and the AR1 of CO_2 concentrations changed between 1981 and 2018. Theil–Sen slopes were also used to calculate trends in CO_2 amplitude, its PV and their AR1.

Drivers of NBP. We used temperature and precipitation data from the Climatic Research Unit TS4.03 dataset[35] to calculate mean annual temperature (MAT), mean annual precipitation (MAP), their temporal variabilities (MAT_{PV} and MAP_{PV}, average of interannual monthly temporal variability), their monthly temporal autocorrelations (MAT_{AR1} and MAP_{AR1}), as well as the temporal trends of all these metrics (ΔMAT, ΔMAP, ΔMAT_{PV}, ΔMAP_{PV}, ΔMAT_{AR1} and ΔMAP_{AR1}) for each pixel following the same procedure established for NBP (see above). To investigate the controls of the spatial variability in aggregated trends in NBP_{PV-AR1}, we also calculated the aggregated indices for ΔMAT_{PV-AR1} and ΔMAP_{PV-AR1} following the same methodology used for NBP (see above). Land-use changes were extracted from land-use harmonization[2] maps (LUH2, http://luh.umd.edu/data.shtml). We calculated the percentage coverages of forests, croplands and urban areas per pixel and the change in these percentages between 1981 and 2015. We calculated mean total atmospheric N deposition per pixel derived from ref. [34], covering the study period. Biodiversity data were extracted from an interpolated gridded global map of vascular plant biodiversity[33], providing one datum per pixel including information on the current number of vascular plant species. We could not include the effects of biodiversity loss in our analyses because global gridded time series of plant biodiversity are not available.

Statistical analyses

We determined how NBP, NBP_{PV}, NBP_{AR1} and their trends (ΔNBP, ΔNBP_{PV}, ΔNBP_{AR1} and the combined ΔNBP_{PV-AR1}) were spatially correlated with

their drivers using spatial generalized linear mixed models with a Leroux conditional autoregressive prior[57] and the S.CARleroux function in the CARBayes R package[58]. All response variables had one datum per pixel, representing aggregated information over the entire study period (for example, NBP indicates mean annual NBP from 1981 to 2018). Models predicting spatial variability in NBP, NBP_{PV} and NBP_{AR1} included biodiversity as a second-order polynomial function to account for the nonlinearities usually found between biodiversity and productivity[59] (biodiversity + biodiversity^2), mean atmospheric N deposition, the interaction between biodiversity and N deposition and the percentages of the area covered by forests and agricultural and urban areas as predictors. MAT and MAP were also included for NBP models, MAT_{PV} and MAP_{PV} for NBP_{PV} models and MAT_{AR1} and MAP_{AR1} for NBP_{AR1} models. We built an extra model including the interaction between biodiversity and mean and variability in climate (biodiversity:MAT + biodiversity:MAP + biodiversity:MAT_{PV} + biodiversity:MAP_{PV}) and the interactions MAT:MAP and MAT_{PV}:MAP_{PV} to further test that the relationship between NBP and biodiversity was not spuriously emerging owing to its relationship with climate (Supplementary information—model summaries, section 8). As indicated by our results, our analyses were able to successfully discern the effect of biodiversity from that of climate (Fig. 3). The fact that the relationship between mean NBP and biodiversity emerging from inversions and the TRENDY ensemble (with no parameterization for biodiversity) were substantially different increases the likelihood of this relationship not being spurious. Models predicting ΔNBP also included the trends in MAT and MAP and the trends in land-use change as predictors. Similarly, models predicting $ΔNBP_{PV}$ and $ΔNBP_{AR1}$ included trends in temperature and precipitation (ΔMAT and ΔMAP) and their temporal variability ($ΔMAT_{PV}$ and $ΔMAP_{PV}$) or autocorrelation ($ΔMAT_{AR1}$ and $ΔMAP_{AR1}$) and trends in land-use changes but not average MAT or MAP or their temporal variability or autocorrelation. Models predicting the combined trends of $ΔNBP_{PV-AR1}$ included a second-order biodiversity as a second-order polynomial, N deposition, average and trends in climate, the aggregated trends of MAT_{PV-AR1} and MAP_{PV-AR1}, average land use and its temporal trends. We additionally tested whether NBP and ΔNBP were spatially related to increasing $ΔNBP_{PV-AR1}$ by fitting two models in which NBP and ΔNBP were the response variables and the aggregated metric of trends in $ΔNBP_{PV-AR1}$ (see description above) was their predictor. Models were fitted using normalized variables (mean = 0, s.d. = 1) but effect plots were rescaled to their original units to facilitate the interpretation of the results. All analyses were performed using R statistical software v.3.6.3 (ref. [60]).

Data availability

Data supporting the findings of this study are available in the following open repositories: CAMS (https://ads.atmosphere.copernicus.eu/cdsapp#!/dataset/cams-global-greenhouse-gas-inversion);CarboScope (http://www.bgc-jena.mpg.de/CarboScope/);and atmospheric CO_2 concentration (https://scrippsco2.ucsd.edu/data/atmospheric_co2/). Data from the TRENDY ensembles can be provided on request from https://globalcarbonbudgetdata.org/. Data to perform the statistical analyses, calculations and figures are publicly available at Figshare: https://doi.org/10.6084/m9.figshare.17081717.v5. Source data are provided with this paper.

Code availability

Code and data to perform the statistical analyses, calculations and figures are publicly available at Figshare: https://doi.org/10.6084/m9.figshare.17081717.v5.

47. Chevallier, F. et al. CO_2 surface fluxes at grid point scale estimated from a global 21 year reanalysis of atmospheric measurements. *J. Geophys. Res.* **115**, D21307 (2010).
48. Chevallier, F. et al. Toward robust and consistent regional CO_2 flux estimates from in situ and spaceborne measurements of atmospheric CO_2. *Geophys. Res. Lett.* **41**, 1065–1070 (2014).
49. Rödenbeck, C., Houweling, S., Gloor, M. & Heimann, M. CO_2 flux history 1982–2001 inferred from atmospheric data using a global inversion of atmospheric transport. *Atmos. Chem. Phys.* **3**, 1919–1964 (2003).
50. Rödenbeck, C., Zaehle, S., Keeling, R. & Heimann, M. How does the terrestrial carbon exchange respond to interannual climatic variations? A quantification based on atmospheric CO_2 data. *Biogeosciences* **15**, 2481–2498 (2018).
51. Sitch, S. et al. Recent trends and drivers of regional sources and sinks of carbon dioxide. *Biogeosciences* **12**, 653–679 (2015).
52. Fernández-Martínez, M. & Peñuelas, J. Measuring temporal patterns in ecology: the case of mast seeding. *Ecol. Evol.* **11**, 2990–2996 (2021).
53. Wood, S. N. *Generalized Additive Models: An introduction with R* 2nd edn (Chapman and Hall/CRC, 2017).
54. Ohlson, J. A. & Kim, S. *Linear Valuation Without OLS: The Theil–Sen Estimation Approach* (SSRN, 2015); https://ssrn.com/abstract=2276927.
55. Komsta, L. Package mblm, 0.12.1: Median-based linear models (2013).
56. Keeling, C. D. et al. in *A History of Atmospheric CO_2 and its effects on Plants, Animals, and Ecosystems* (eds Ehleringer, J. R. et al.) 83–113 (Springer Verlag, 2005).
57. Leroux, B. G., Lei, X. & Breslow, N. in *Statistical Models in Epidemiology, the Environment and Clinical Trials* (eds Halloran, M. & Berry, D.) 179–191 (Springer-Verlag, 2000).
58. Lee, D. CARBayes: an R package for Bayesian spatial modeling with conditional autoregressive priors. *J. Stat. Softw.* **55**, 1–24 (2013).
59. Gonzalez, A. et al. Scaling-up biodiversity–ecosystem functioning research. *Ecol. Lett.* **15**, ele.13456 (2020).
60. R Core Team. *R: A Language and Environment for Statistical Computing* (R Foundation for Statistical Computing, 2020).

Author contributions M.F.-M., J.P. and I.A.J. planned and designed the research. F.C., C.R., S.S., P.F., V.A., D.G., A.K.J., D.L.L. and P.C.M. provided the data. M.F.-M. analysed the data. All previously mentioned authors, along with P.C., M.O., J.S., S.V. and H.Y., contributed substantially to the writing of the manuscript.